OSIP1 is a self-assembling DUF3129 protein required to protect fungal cells from toxins and stressors

Nicolas Valette, Julien Renou, Alexis Boutilliat, Antonio José Fernández-gonzález, Valérie Gautier, Philippe Silar, Christophe Guyeux, Jean-claude Charr, Stéphane Cuenot, Christophe Rose, et al.

OSIP1 is a self-assembling DUF3129 protein required to protect fungal cells from toxins and stressors

Running title: OSIP1 prevent cell wall stress

Nicolas Valette[a], Julien Renou[a], Alexis Boutilliat[a], Antonio José Fernández-González[a], Valérie Gautier[b], Philippe Silar[b], Christophe Guyeux[c], Jean-Claude Charr[c], Stéphane Cuenot[d], Christophe Rose, Eric Gelhaye[a], Mélanie Morel-Rouhier[a#].

[a]Université de Lorraine, INRAe, Interactions Arbres/Micro-organismes (IAM), UMR 1136, F-54000 Nancy, France

[b]Université Paris Diderot, Sorbonne Paris Cité, Laboratoire Interdisciplinaire des Energies de Demain (LIED), 75205 Paris, France

[c]Computer Science Department, FEMTO-ST Institute, UMR 6174 CNRS, Université de Bourgogne Franche-Comté, 16 route de Gray, 25030 Besançon, France

[d]Institut des Matériaux Jean Rouxel, Université de Nantes, 2 rue de la Houssinière, 44322 Nantes Cedex 3, France

[e] Université de Lorraine, AgroParisTech, INRAE, UMR Silva, Nancy, 54000, France.

[#]**Corresponding author:** Mélanie Morel-Rouhier, Université de Lorraine, UMR1136 INRA-Université de Lorraine "Interactions Arbres/Micro-organismes", Faculté des Sciences et Technologies BP 70239, F-54506 Vandoeuvre-lès-Nancy Cedex, France. Melanie.Morel@univ-lorraine.fr, phone: +33 3 72 74 51 62.

Keywords: OSIP1, fungi, cell wall, stress, oak extractives, secretome

Summary (200 mots)

Secreted proteins are key players in fungal physiology and cell protection against external stressing agents and antifungals. OSIP1 is a fungal-specific protein with unknown function. By using *Podospora anserina* and *Phanerochaete chrysosporium* as models, we combined both *in vivo* functional approaches and biophysical characterization of OSIP1 recombinant protein. Our data showed an increased sensitivity of the *P. anserina OSIP1*$^{\Delta}$ mutant to both caspofungin and oak-extractives. This correlated with the weakened extracellular matrix produced by the mutant compared to the wild type, as highlighted by SEM imaging. This alteration quantitatively modified the global secretome of *P. anserina* grown in presence of wood, such as proteins associated to the cell-wall integrity signaling pathway. Since the recombinant OSIP1 form *P. chrysosporium* self-assembled as fibers and was capable of gelation, these results argue for a structural role of OSIP1 proteins in fungi at the cell wall or within the matrix confering cell protection against external toxic compounds. These data could be of great interest for increasing protein secretion in a context of lignocellulosic biomass degradation, such as improving the efficiency of antifungals that could be trapped within the extracellular matrix.

Introduction

During evolution, fungi had to adapt to environmental constraints. The secretome, *i.e*. the proteins secreted in the extracellular medium, is a good marker of fungal physiology and trophic modes. Indeed, the secretome is involved in the first steps of the symbiosis or infection establishment and plays essential roles in plant biomass degradation (Kämper *et al.*, 2006; Bouws *et al.*, 2008; Vincent *et al.*, 2012). Fungal secretomes are composed of degradative enzymes such as proteases, lipases, Carbohydrate-Active enZymes (CAZymes), and ligninolytic enzymes for some wood-decaying species (Zhu *et al*., 2016; Pellegrin *et al*., 2015). This degradative system has been intensively studied due to its important application in lignocellulose biomass valorization. In plant-associated fungi, other proteins can be secreted to modulate plant immunity and establish symbiosis or allow pathogenic infection (Plett *et al*., 2011; Pazzagli *et al*., 1999; Frias *et al*., 2011; Baccelli *et al*., 2014). Some of them, the hydrophobins, are involved in the attachment of fungal structures to different kinds of surfaces and the development of hyphae at the water/air interface (Wessels *et al*., 1991; Wessels, 1996). In fungal pathogens, hydrophobins might act as virulence factors to enhance fungal infection (Ruocco *et al*., 2015; Kubicek *et al*., 2008), while in symbiotic associations, these proteins could be involved in mycorrhizae formation (Plett *et al*., 2012). Most of the studied hydrophobins are directed to the extracellular medium through the secretory pathway. However, they often remain associated with the fungal cell wall and can be found inside fruiting bodies and on the surfaces of hyphae, spores and conidia (Dynesen *et al*., 2003; Linder, 2009). Many other secreted proteins have been identified but remain of unknown function. This is the case for SSP (for Small Secreted Proteins with sequence less than 300 amino acids) (Alfaro *et al*., 2014). The percentage of SSP-coding genes in the genomes of saprophytic fungi such as *Phanerochaete chrysoporium*, *Trametes versicolor* or *Aspergillus fumigatus* is similar to the one of the ectomycorrhizal fungus *Laccaria bicolor* (between 2 and

3 % of the predicted gene models) (Pellegrin *et al*., 2015; Valette *et al*., 2016). At the protein level, SSPs represent between 4 and 12% of the proteins identified in the secretomes of various *Aspergillus* species grown on sugar beet pulp or wheat bran (Valette *et al*., 2016). However, only few have been functionally characterized. One SSP of the lignolytic fungus *Pleurotus ostreatus* is involved in the regulation of the lignolytic system by modulating expression and activity of aryl-alcohol oxidases, aryl-alcohol dehydrogenases and versatile peroxidases (Feldman *et al*., 2017) and in the transition from primary to secondary metabolism, development, aging, and fruiting body initiation (Feldman *et al*., 2019).

In a previous analysis, we have highlighted the up-regulation of various SSP-coding genes of the lignolytic fungus *Phanerochaete chrysosporium* in presence of oak extractives (Thuillier *et al*., 2014, Fernández-González *et al*., 2018). Oak extractives are mainly composed of phenolic compounds and flavonoids (Zhang *et al*., 2015; Fernández-González *et al*., 2018). These molecules are released from wood during the degradative process and can be toxic for cells by various mechanisms such as metal and free radical scavenging activity, direct interaction with enzymes, perturbation of ionic homeostasis and disruption of membrane and cell wall integrity (Valette *et al*., 2017). One of these up-regulated genes retained our attention because the corresponding protein was also detected at high amount in the secretome of another white rot fungus *Trametes versicolor* grown on oak wood chips (Deroy et al., unpublished). This protein was thus named OSIP1 for Oak Stress Induced Protein. It shows no sequence homology with characterized proteins in the databases. In this study we used two fungal models to decipher the role of OSIP1: *Podospora anserina* for functional analysis because genetic engineering is easy, contrary to *P. chrysosporium* or *T. versicolor;* and *P. chrysoporium* for the biochemical analysis because only PcOSIP1 was successfully produced as a recombinant protein.

Results

Comparative genomic analysis reveals that OSIP1 is widespread in fungi

OSIP1 sequences from the ascomycete *P. anserina* (*PaOSIP1*: ProtID JGI 208230, a.k.a. Pa_5_3780 according to the *P. anserina* genome project) and the basidiomycete *P. chrysosporium* (*PcOSIP1:* ProtID JGI 2981896) were used as templates to search for fungal sequences using the BlastP search tool onto the whole fungal JGI database (Mycocosm from Joint Genome Institute). The sequence of *P. anserina P209725* (ProtID JGI 209725) was also used as template since it displays 38% similarity with *PaOSIP1*). A total of 1057 protein sequences were retrieved and analyzed by clustering. These sequences grouped into nine clusters (Fig. 1A). *PaOSIP1* and *PcOSIP1* belonging to cluster 1, this latter was thus named OSIP1 cluster (species and accession numbers are available in Table S1). It gathers sequences from both ascomycetes (*Pezizomycotina*) and basidiomycetes (*Agaricomycotina* and *Pucciniomycotina*). Moreover, this analysis revealed that *OSIP1* is present in genomes of wood decay fungi, and also in mycorrhizal, pathogenic fungi and other saprotrophs (Fig. 1A). Although OSIP1 was found induced by oak extractives in lignolytic fungi (Thuillier *et al*., 2014; Deroy, unpublished), this genomic analysis showing that OSIP1 is present in fungi with various trophic modes, argues against its direct involvement in the lignolytic process and suggests a more general role in fungal physiology.

OSIP1 sequences contain a DUF3129 domain, like some appressoria-specific proteins

OSIP1 sequences exhibit a signal peptide of secretion, a conserved DUF3129 domain and a variable C-terminal tail (Fig. 1B). In ascomycetes, 8 cysteinyl residues are conserved, while only four have been detected in the analyzed basidiomycete sequences (Fig. 1B and Fig S1). The DUF3129 domain is not restricted to OSIP1 sequences. It can be identified in both ascomycetes and basidiomycetes and was retrieved in 442 sequences from the Pfam 31.0

database. Although most of the proteins having the DUF3129 are annotated as uncharacterized proteins, some of them are described as being related to CAS1 (*Colletotrichum gloeosporioides* appressoria-specific protein), MAS (*Magnaporthe* appressoria-specific protein), gEgh16 from *Blumeria graminis* proteins, all being putatively involved in fungal cell wall remodeling. A phylogenetic analysis was performed with the sequences from the OSIP1 cluster and the 442 sequences containing the DUF3129 domain (Fig. 1C). PaOSIP1 clusters with ascomycete sequences but independently of CAS1 from *C. gloeosporioides*, MAS3 from *M. grisea* and gEgh16 from *B. graminis*. Among basidiomycetes, sequences from *Agaricomycotina* with lignolytic, saprotrophic or mycorrhizal lifestyles (Group A) cluster independently from sequences of pathogenic basidiomycetes from *Pucciniomycotina* and *Agaricomycotina* (Group B) (details are given in Table S1).

PaOSIP1 maintains cell wall integrity under caspofungin stress

To functionally characterize OSIP1, the OSIP1 knock-out mutant was generated in *P. anserina* (*PaOSIP1*$^{\Delta}$) (Fig S2). *PaOSIP1*$^{\Delta}$ was tested for its ability to grow on various carbon sources (cellobiose, fructose, cellulose, pectin, glucose) and various biomasses (whatman paper, hay, miscanthus, wood chips). No differences in growth, sporulation, nor appressoria-like structure formation (as described in Brun *et al*., 2009) was highlighted between the wild type and the *PaOSIP1*$^{\Delta}$ mutant strains in the tested conditions (data not shown). Because the DUF3129 domain is present in cell wall remodeling proteins, cell wall destabilizing agents were thus tested. No phenotype was observed for Congo red that prevents glucan microfibril assembly mainly by binding β-1,3 glucans (Nodet *et al*., 1990) nor Calcofluor white, which binds chitin. By contrast, a significant deleterious growth phenotype was observed for the mutant compared to the wild type in presence of caspofungin (Fig. 2). Caspofungin is a cell

wall-targeting antifungal compound extensively used in clinical settings for the treatment of infections caused by diverse fungi. Caspofungin inhibits the synthesis of β-1,3-glucan, a crucial cell wall component for many fungi, by targeting the β-1,3-glucan synthase (encoded by *fks1*) in a non-competitive way (Van Den Bossche, 2002; Aguilar-Zapata *et al*., 2015). Functional complementation of *PaOSIP1*$^{\Delta}$ by PaOSIP1 restored the growth defect confirming the role of PaOSIP1 in protecting cell wall under caspofungin treatment.

PaOSIP1$^{\Delta}$ mutant is affected in extracellular matrix production

To check whether caspofungin sensitivity was due to a thinner cell wall in the mutant compared to the wild type, SEM imaging was performed after cryosection of the hyphae (Fig. 3). The whole reconstituted images are shown as supplementary data. The thickness of the cell wall was measured (n>50) based on the microscopic images. No difference was detected between the WT and the mutant, nor between the caspofungin and the control condition. The measured cell wall thickness of hyphae cross-sections was around 150 nm for all conditions analysed. Interestingly, the main difference highlighted by comparing SEM images of both mutant and WT strains was the extracellular matrix (ECM) density. Fungal extracellular matrix is mainly composed of carbohydrates and proteins in complex interactions. This matrix is strongly reduced in *PaOSIP1*$^{\Delta}$ even in the absence of caspofungin (Fig. 3). Since this matrix was shown to prevent drugs from reaching their cellular targets (Mitchell *et al*., 2016), this could explain why *PaOSIP1*$^{\Delta}$ showed an increased sensitivity to the antifungal caspofungin.

Recombinant OSIP1 self-assembles as fibers and forms a gel

The heterologous *Escherichia coli* system was tested for recombinant PaOSIP1 and PcOSIP1 productions. Only PcOSIP1 expressed in *E. coli* was successfully produced. After

purification, 3 mg of pure protein per liter of bacterial culture were obtained. To check whether the protein was correctly folded, far-UV circular dichroism analysis was performed. Spectrum of PcOSIP1 revealed secondary structures, mainly alpha helices as highlighted by a positive band at 190 nm and two negative bands at 208 and 222 nm (Fig. 4A).

After purification, PcOSIP1 rapidly self-assembled as big oligomers in Tris-NaCl buffer (30 mM Tris-HCl pH 8.0, 200 mM NaCl), as shown by dynamic light scattering (DLS) analysis (Fig. 4B). Huge hydrodynamic radii (Rh) of 789.3 ± 388 nm and 2 281 ± 880 nm were respectively measured for 56.7% and 28.7% of the PcOSIP1. This aggregation was not observed when the protein was dialyzed in 50 mM phosphate buffer pH 8.0 directly after purification, suggesting that this process was driven by the physicochemical properties of the buffer. To check whether this aggregation was due to protein instability and thus precipitation or rather a specific organization, the macromolecular structures of PcOSIP1 was analyzed by Atomic Force Microscopy (AFM). In Tris-NaCl buffer, PcOSIP1 was able to self-assemble into fibers with a mean diameter of 1.5 ± 0.2 nm (Fig. 4C). In phosphate buffer, a crown structure was evidenced. This crown organization could be the transient states of PcOSIP1 fibril formation, since such structure was already described in transient states of the human α-synuclein fibril formation that contributes to Parkinson's disease (Lashuel *et al*., 2002 ; Apetri *et al*., 2006).

All the experiments described above were performed directly or few days after protein purification. Interestingly, storing PcOSIP1 in Tris-NaCl buffer in the freezer led to the formation of a gel, that was quite compact and elastic (Fig. 4D). This specific feature was already described for other proteins as α-synuclein that can form gels in buffer at pH 7.4 in the presence of NaCl (Semerdzhiev *et al*., 2018). These atypical properties of self-assembly and jelly structure formation support a putative structural role of OSIP1 protein within the fungal cell wall or the extracellular matrix.

Oak-extractives affect *PaOSIP1*$^{\Delta}$ growth

During wood degradation, extractives act as important stressors for fungal cells (Thuillier *et al*., 2014 ; Valette *et al*., 2017 ; Fernández-González *et al*., 2018). Some of them can act directly on cell wall integrity. For example, similarly to caspofungin, cinnamaldehyde and poacic acid inhibit β-1,3-glucan synthesis within the fungal cell wall (Bang *et al*., 2000; Piotrowski *et al*., 2015). Because OSIP1 gene expression was induced by oak extractive-induced stress both in *P. chrysosporium* (Thuillier *et al*., 2014) and *P. anserina* (data not shown), this condition was used to test *PaOSIP1*$^{\Delta}$ growth phenotype. The results showed a growth delay of *PaOSIP1*$^{\Delta}$ compared to the wild type in presence of wood extractives, which was observable from 5 days (Fig. 5). This phenotype was partially restored by functional complementation with PaOSIP1. These results support the hypothesis that PaOSIP1 could participate in cell wall protection against extractives toxicity.

The deletion of OSIP1 strongly modifies the composition of the secretome and the cell-wall related proteins of *P. anserina* in presence of oak sawdust

To analyze how the deletion of PaOSIP1 affects the fungal physiology in a context of biomass degradation, a proteomic analysis was performed for the *PaOSIP1*$^{\Delta}$ mutant grown in presence of oak sawdust, in comparison with the wild type strain. The comparative analysis of the secreted proteins reveals strong modification of the global secretome of *PaOSIP1*$^{\Delta}$ mutant compared to the wild type strain (Fig. 6A). Indeed, over the 250 proteins detected, 150 were more abundant (Protein abundance index (PAI) fold>2) or specifically identified in the mutant compared to the wild type, while this number was only 41 in the case of the wild type.

By looking at the various classes of enzymes that were more abundant in the mutant secretome compared to the WT, no clear specificity was observed except for proteases that

were less represented (Fig. 6B). Globally, more than half (around 60%) of the detected proteins of a specific class were more abundant in the secretome of the mutant compared to the wild type. It is likely that the deletion of OSIP1 globally affected the secretion process of the enzymes.

Glycoside hydrolases (GH) were the most abundant proteins with a total of 66 GH detected in both secretomes. By looking at the individual GH families, we showed again that the increase in protein abundance is not restricted to specific families, but was observed for many of them (Fig. 6C). However, it is interesting to note that 16 GH families (over the total of 29) were specifically detected in the mutant strain, especially GH5, GH11 and GH43 with at least 3 isoforms.

A high number of cell wall-related proteins, in particular glucan-acting enzymes have also been found more abundant in the secretome of the mutant strain (Fig. 6D). Moreover, many Wall Stress responsive Component (WSC) proteins have been detected. These proteins serve as sensors of external stress cues upstream of cell wall integrity (CWI) pathway in *Saccharomyces cerevisiae* (Verna *et al*., 1997) and *Aspergilli* (Futagami *et al.*, 2011; Dichtl *et al*., 2012). In line with this observation, respectively 3 and 6 DUF1996-containing proteins were found more abundant and specifically detected in the mutant among the 10 detected in total (Supplementary data). These proteins are of unknown function, however the DUF1996 domain has been associated to fungal stress sensing and response (Tong *et al*., 2016a and 2019).

Discussion

In this study, we characterized a new fungal protein, which participates in cell wall fitness under stress. The comparative genomic analysis revealed that such proteins are widely present in fungi, suggesting their involvement in a general process of stress rescue. All analyzed

OSIP1 possess a domain of unknown function DUF3129 that was previously identified by few studies in proteins of both plant and insect pathogens (Shang *et al*., 2016). DUF3129 is an expanded gene family highly expressed during infection in nematode-trapping fungi that form adhesive branches and adhesive knobs (Andersson *et al*., 2014). The role of this domain was attributed to the cell wall remodeling for fungal penetration to host cuticules with an unclear mechanism (Justesen *et al*., 1996 ; Xue *et al*., 2002 ; Grell *et al*., 2003 ; Cao *et al*., 2012). More recently, seven DUF3129 proteins of the insect pathogenic fungus *Metarhizium robertsii* were found localized to cellular lipid droplets mediating their degradation and subsequently controlling appressorial turgor required for infection (Huang *et al*., 2019). However, nothing has been described concerning the role of these DUF3129-containing proteins in saprophytic fungi. The jelly structure of the recombinant PcOSIP1 and the reduction of the extracellular polysaccharide network observed for the PaOSIP1 mutant strongly suggest the involvement of OSIP1 in the formation of such adhesive structures in fungi. The weakened extracellular matrix of the mutant could thus be responsible for the higher susceptibility of the fungus to both caspofungin and oak extractives.

This phenomenom has been already described in *A. fumigatus*, where the downregulation of a hydrophobin gene by a polyphenolic compound resulted in a weakened extracellular matrix and therefore increased the susceptibility of the fungi to antifungal drugs (Luo *et al*., 2018). Hydrophobins are small (100–120 aa) secreted proteins characterized by the presence of eight highly conserved cysteine residues and the ability to self-assemble as amyloid-like structure and forms rodlets (Ball *et al*., 2020). Amyloids serve diverse purposes for structure, adhesion and defence in microorganisms (Shanmugam *et al*., 2019) and can be evidenced *in vitro* using fluorescent tool as thioflavin T, which binds to the beta sheet-rich structure characteristic of amyloid-like structure (Groenning, 2010). PcOSIP1 does not assemble under amyloid structure since no thioflavin T fluorescence signal was detected in any of the conditions of

temperatures and buffers tested (data not shown). We have shown that PcOSIP1 was rich in α-helices, while amyloid is structurally dominated by β-sheets. Moreover, AFM revealed that it did not form rodlets. These experimental data, coupled to sequence analysis, allowed us to confirm that OSIP1 is a new self-assembling protein, that does not belong to the well-known class of hydrophobins.

In the context of lignocellulosic biomass degradation, the structural property of OSIP1 may be the key point explaining the way by which it participates in fungal stress resistance by protecting the cell wall. In accordance, the comparative secretome analysis of *P. anserina* grown on oak sawdust revealed that the *PaOSIP1*$^{\Delta}$ mutant highly expresses WSC proteins compared to the wild type in this condition. WSC proteins are localized to the cell wall and the plasma membrane and act as sensors upstream of the cell-wall integrity pathway. In particular, WSC-1 may function in regulating cell wall biogenesis through the MAK-1 pathway in *Neurospora crassa* (Maddi *et al*., 2012). Single deletions of the five wsc genes of *Beauveria bassiana* resulted in significant, but differential, increases in cellular sensitivity to cell wall perturbation, oxidation, high osmolarity, and metal ions (Tong *et al*., 2016b). In *Aspergillus fumigatus*, deletions of *wsc1* caused an increased in sensitivity to caspofungin but no change in cellular sensitivity to other cell wall perturbation, alkaline pH and high temperature (Dichtl *et al*., 2012). In the nematode-trapping fungus *Monacrosporium haptotylum*, a gene cluster of 5 secreted proteins that are adjacent in the *M. haptotylum* genome (cluster 74) is highly (>10-fold) upregulated during infection (Andersson *et al*., 2013). This cluster gathers two genes coding for WSC proteins, one gene containing the DUF3129 domain and two SSP-coding genes (Meerupati *et al*., 2013). This suggests a functional link between these proteins. Additionally to WSC proteins, the *PaOSIP1*$^{\Delta}$ mutant highly expresses DUF1996-containing proteins. In *B. bassiana*, DUF1996-containing proteins localize in vacuoles and play significant roles in the response to cell-wall perturbation, high

osmolarity, oxidation, fungicidal and multiple metal stress (Tong *et al*., 2016a). The absence of OSIP1 in *P. anserina* grown in presence of oak sawdust strongly affected the whole secretome of the fungus, likely because of the cell wall weakness. Indeed, the functionality of the cell wall integrity (CWI) and secretory systems are connected and coordinately respond to exogenous stresses through the modulation of the cell periphery and secretion (Malavazi *et al*., 2014).

Taking together, these data strongly suggest that OSIP1 proteins prevent cell wall stress. Consequently, its absence affects the cell wall associated signaling pathway, leading to a deregulation of the secretion process. These data could be of great interest for both the improvement of protein secretion particularly in a context of lignocellulosic biomass degradation, and the limitation of fungal pathogenicity, for which the fungal cell wall has a crucial role (Gow *et al*., 2017).

Experimental procedures

Growth conditions

The *P. anserina* strain used in this study was derived from the S strain (Rizet, 1952; Boucher *et al*., 2017). Standard culture conditions, media compositions and genetic methods for this fungus have already been described (Rizet, 1941; Silar, 2013) and are available at https://podospora.i2bc.paris-saclay.fr. Growth kinetics of the wild type and *PaOSIP1*$^{\Delta}$ strains were done in M2-Agar medium and M2-Agar medium supplemented with caspofungin (500 ng/ml) and oak extractives (2 mg/ml) for 10 days at 27 °C. Oak (*Quercus petraea*) acetonic extract preparation has been performed as described previously (Fernández-González *et al*., 2018).

Analysis of OSIP1 sequences

OSIP1 sequences were searched within all fungal genomes available in the Joint Genome Institute database (Mycocosm https://genome.jgi.doe.gov/programs/fungi/index.jsf) using BlastP with a cut off of Evalue=10^{-5}. Sequences of OSIP1 of *Podospora anserina* ((PaOSIP1 (208230 JGI) and *Phanerochaete chrysosporium* (ProtID 2981896 JGI) have been used as templates. Another sequence close to PaOSIP1 was added as a template (P209725 (ProtID 209725 JGI)). Evolutionary analyses were conducted in MEGA7 using the Neighbor-Joining method (Kumar *et al*., 2016). The tree is drawn to scale, with branch lengths in the same units as those of the evolutionary distances used to infer the phylogenetic tree. The evolutionary distances were computed using the Poisson correction method and are in the units of the number of amino acid substitutions per site. The analysis involved 628 amino acid sequences. All ambiguous positions were removed for each sequence pair. There were a total of 467 positions in the final dataset. To carry out the clustering, the Laplacian eigenmap technique (Belkin and Niyogi, 2003) was applied with Gaussian mixture model (Reynolds, 2015) as follows. After sorting the sequences in alphabetical order, the similarity of each sequence pair were obtained from the score provided during a pairwise sequence alignment using the Needleman-Wunsch (Needleman and Wunsch, 1970) dynamic programming algorithm from Biopython (Cock *et al*., 2009) module (pairwise2 function). Default values for gap open and extend penalties were chosen with blosum62 matrix for amino acid substitution, leading to a matrix M of integers. A similarity matrix S has been deduced by dividing each row by its maximum, and by computing the identity matrix minus this one. The normalized Laplacian associated with the similarity matrix has been computed as follows: $L = D^{-1}(D-S)$, where D is the diagonal matrix whose element in position (i,i) is the sum of the i-th row in S. Eigenvalues of L have then been computed and sorted in ascending order thanks to the numpy library (Oliphant, 2006), and the N-th first eigenvalues have only be considered, where N is such that the increase between the N-th and N+1-th eigenvalue is lower than 1%. Associated

eigenvectors have then been clusterized according to a Gaussian mixture model (Reynolds, 2015), and the model selection (number of Gaussians) has been performed according to the Bayesian Information Criterion (BIC, (Schwarz, 1978)). To sum up, Laplacian eigenmap allowed us to map the similarity matrix in a low dimensional space of points, each point being associated to one amino acid sequence. This cloud points has been considered as the superposition of a given number of gaussian trends (the clusters), this number being determined thanks to the BIC criterion of parcimony. For further information about this sequence clustering technique, see, e.g. Bruneau *et al*. (2018).

Deletion of PaOSIP1 in *Podospora anserina*

To delete PaOSIP1 (Pa_5_3780), the "split marker" method was used (Silar, 2013). This protocol is based on the generation of two DNA fragments carrying a resistance marker flanked with either 5' or 3' non-coding sequence of the genes by two successive PCR reactions. In the first step, a 832 pb-long 5'-non-coding region of PaOSIP1 and a 962 pb-long 3' region were PCR-amplified from the S strain DNA with the PaOSIP1-A/ PaOSIP1-B, and PaOSIP1-C/ PaOSIP1-D primer pairs respectively. At the same time, the hygromycin resistance marker was amplified with PaOSIP1-E and PaOSIP1-F from the pBC-hygro vector (Silar, 1995). Primers sequences are given in Fig. S2. In a second step, the second round of PCR using primers PaOSIP1-A and PaOSIP1-F, and PaOSIP1-D and PaOSIP1-E enabled to merge the resistance marker with either the 5' or the 3' region. The two PCR products were used to transform a mus51::phleoRstrain, in which the mus51gene encoding one of the subunit of the non-homologous end joining dimer is replaced with a phleomycin resistance gene. Three crossing-over events between the two cassettes and the *P. anserina* genome enabled the deletion of PaOSIP1. Three hygromycin resistant transformants were selected. They were crossed with the wild-type S strain, and one homokaryotic hygromycin resistant

and phleomycin-sensitive descendant was selected as the PaOSIP1::hygroRstrain or *PaOSIP1*$^{\Delta}$. Its genotype was confirmed by Southern blot analyses using digoxigenin labeled probes (Fig. S2). For functional complementation tests, PaOSIP1 coding sequence was cloned into pAKS-Genet^{R} vector and expressed in *PaOSIP1*$^{\Delta}$. The presence of the gene was checked by PCR and three transformants were selected for functional complementation tests. They all restored the mutant phenotype, thus, only the results for one of them are presented.

SEM imaging of *PaOSIP1*$^{\Delta}$ hyphal network

Cloning of PcOSIP1

Phanerochaete chrysosporium mycelium was harvested from liquid cultures in TK medium supplemented with oak extractives as previously described (Thuillier *et al*., 2014). Total RNA was extracted and purified using the RNeasy plant minikit (Qiagen) according to the manufacturer's instructions. RNA was treated with DNase I during purification as recommended in the manufacturer's protocol. An additional purification step was performed by precipitating RNA with 2 M LiCl. RNAs were reverse transcribed using the masterscript kit (5 prime) following the manufacturer's protocol. The PCR reactions to amplify PcOSIP1 (Prot ID 2981896 in the Joint Genome Institute database v2.2 (previously identified as Prot ID 4474 in v2.0 of *P. chrysosporium* genome annotation)), have been performed with Herculase Taq (Agilent technologies) for cloning into the pEt26b (Novagen) vector for His-tagged protein production in *Escherichia coli.* The sequence was amplified without the predicted signal peptide of secretion using the following primers (for: CCCCCATATGGCTATTATCACGCCCGCG and rev: CCCCGCGGCCGCTGCTTGGAGCTCCTCATC).

Heterologous expression of PcOSIP1 in *Escherichia coli* and purification of the recombinant protein

Expression of recombinant PcOSIP1 was performed in *E. coli* Rosetta2 (DE3) strain containing pLysS plasmid (F^- ompT $hsdS_B$(rB– mB–) gal dcm (DE3) pRARE2 (CamR)). The bacteria were cultivated in LB medium supplemented with 50µg/ml kanamycin and 50µg/ml chloramphenicol at 37°C. At OD_{600} of 0.6, the expression of the recombinant proteins was induced by adding 0.1 mM isopropyl ß-D-1 thiogalactopyranoside (IPTG) during 4h. Cells were harvested by centrifugation and resuspended in 30 mM Tris-HCl pH 8.0, 500 mM NaCl buffer and stored at -20°C. The purification of His-tagged PcOSIP1 was performed by affinity chromatography on IMAC columns (Sigma Aldrich) from the soluble fraction obtained after a 30 min centrifugation (27,000 x g) of cells lysed by sonication. The washing buffer was 30 mM Tris–HCl pH 8.0, 2 M NaCl in a first step and 30 mM Tris–HCl pH 8.0, 500 mM NaCl and 10 mM imidazole in a second step. The elution buffer was 30 mM Tris–HCl pH 8.0, 500 mM NaCl, 250 mM imidazole. Both proteins were dialyzed against a 30 mM Tris-HCl pH 8.0, 500 mM NaCl buffer by ultrafiltration on YM10 membranes, concentrated and loaded on Sephadex 75 16/600 column (AKTA purifier) equilibrated with 30 mM Tris-HCl, 200 mM NaCl. The purified protein was finally concentrated and analyzed on 15% SDS-PAGE gel to check the purity. The concentration of the protein was determined by BC assay (interchim).

Circular dichroism (CD)

Due to the incompatibility of Tris buffer, which absorbs between 180 and 260 nm, the PcOSIP1 spectrum was recorded exclusively in phosphate buffer. Directly after purification, PcOSIP1 was dialyzed in 50 mM phosphate buffer pH 8.0 using dialysis membrane (Spectra/Por, MWCO 6-8 000). Circular Dichroism spectra of PcOSIP1 was obtained in 50 mM phosphate buffer pH 8.0 at 25 °C in a quartz cuvette (1-mm path length) from 180 to 260

nm with a bandwidth of 1 nm using a Chirascan Plus spectropolarimeter (Applied Photophysics, Ltd, UK). The mean residue ellipticity [θ]MR was calculated using Pro-Data Viewer (Applied Photophysics, Ltd, UK) software and expressed in deg. $cm^2.dmol^{-1}$ per residue.

Dynamic Light Scattering (DLS)

The homogeneity of solutions, the aggregation state and particle sizes were analyzed by granulometry on a Zetasizer Nano-S model (Malvern Instruments, Malvern, UK). The protein solution was analyzed by DLS at a final concentration of 4mg/ml either in 50 mM phosphate buffer pH8.0 or 30 mM Tris-HCl, 200 mM NaCl buffer. The supernatant of each sample was gently transferred into a quartz cuvette of 12 µl and the particle size measurements were performed in triplicate at 37°C, with alight diffusion at 173°. The data were collected in automatic mode and analyzed using the associated software DTS version 4.2 (Malvern Instruments).

Atomic Force Microscopy (AFM)

PcOSIP1, either in 50 mM phosphate buffer (pH 8.0) or 30 mM Tris-HCl and NaCl 200 mM buffer (pH 8.0), was analyzed at a starting protein concentration of 6 mg/ml. The protein solutions were carefully dialyzed to remove NaCl and diluted 10 times just prior to AFM observations. A glass coverslip was cleaned with a piranha treatment and washed in ultrapure water, before being dried in a stream of nitrogen gas. A tiny droplet of each diluted protein solution was deposited onto the glass coverslip heated at 20°C to promote a rapid drying (within 2 minutes) while avoiding the formation of concentration gradients on the substrate (Zykwinska *et al.*, 2014). The sample was then immediately imaged by AFM. A NanoWizard® Atomic Force Microscope (JPK, Germany) operating in intermittent contact

mode under ambient conditions was used to image the protein solutions deposited onto the glass coverslip. A standard rectangular cantilever (Nanosensors NCL-W) was employed for imaging (scan rate of 0.5 Hz), with a free resonance frequency of 174 kHz and a curvature radius of the tip of 10 nm. In order to check the reproducibility of the observed morphology, all samples were scanned at least on three different zones. Each sample was investigated using fresh tips previously cleaned by UV-ozone treatment. The height measurements were done using JPK Data Processing software (JPK, Germany).

LC–MS/MS protein identification

P. anserina wild type and *PaOSIP1*$^{\Delta}$ strains were cultivated in flasks containing 1 g of oak sawdust and 10 ml of M2 medium without any carbon source for 1 month at 25°C. For each strain, three independent cultures were pooled before protein extraction. Proteins from the whole sample (sawdust containing mycelium and secretome) were extracted with 10 ml of 50 mM sodium acetate pH4.5 buffer for 1.5 h under shaking at 4°C. The sample was centrifuged, concentrated with centricon filter membrane (5 kDa) until around 3 ml and precipitated with cold acetone (80%). 10 µg of proteins was loaded on 12% SDS-PAGE gel. After a short migration (0.5 cm) in the stacking gel, the gels were stained with Coomassie blue and each electrophoresis track was cut into two 2-mm-wide strips. Proteomic identification was performed at the Plate-forme d'Analyse Protéomique de Paris Sud-Ouest (PAPPSO, INRA, Jouy-en-Josas, France; http://pappso.inra.fr/), according to a protocol described in Navarro et al. (2010). Briefly, the digestion of the proteins contained in the gel strips was carried out according to a standard trypsinolysis process, using modified trypsin (Promega, Charbonnières-les-Bains, France). Peptide analysis was performed by Ultimate 3000 RSLCnano liquid chromatography (Thermo Fisher Scientific, Waltham, Massachusetts, USA) coupled to a Q-exactive mass spectrometer (Thermo Fisher Scientific) using electrospray

ionization. Peptide attribution and protein annotation were performed by comparing mass spectrometry data to predicted proteins in the genomes of *P. anserina* as well as an internal contaminant database, using X!Tandem Cyclone software (X!Tandem, Jouy-en-Josas, France). The protein annotation was completed manually by BlastP using both the NCBI (https://blast.ncbi.nlm.nih.gov) and JGI Mycocosm (https://mycocosm.jgi.doe.gov/Podan3/Podan3.home.html) databases.

Acknowledgements

This work was supported by a grant overseen by the French National Research Agency (ANR) as part of the "Investissements d'Avenir" program (ANR-11-LABX-0002-01, Lab of Excellence ARBRE) and the Region Lorraine Research Council. We thank Thomas Bacchetta for experimental help, Sylvie Cangemi for expert technical assistance, Christophe Rose (UMR SILVA-SILVATECH INRAE) for microscopy and Alexandre Kriznik for CD data (UMR7365 UL/CNRS IMoPA, Nancy, France). Proteomics analyses were performed on the PAPPSO platform (http://pappso.inra.fr) which is supported by INRA (http://www.inra.fr), the Ile-de-France regional council (https://www.iledefrance.fr/education-recherche), IBiSA (https://www.ibisa.net) and CNRS (http://www.cnrs.fr).

The authors declare no competing interests.

References

Aguilar-Zapata, D., Petraitiene, R., and Petraitis, V. (2015) Echinocandins: The Expanding Antifungal Armamentarium. Clin Infect Dis 61 Suppl 6:S604-11.

493 Alfaro, M., Oguiza, J.A., Ramírez, L., and Pisabarro, A.G. (2014) Comparative analysis of
494 secretomes in basidiomycete fungi. J Proteomics 102: 28–43.
495
496 Andersson, K.M., Meerupati, T., Levander, F., Friman, E., Ahrén, D., and Tunlid, A. (2013)
497 Proteome of the nematode-trapping cells of the fungus *Monacrosporium haptotylum*. Appl
498 Environ Microbiol 79: 4993-5004.
499
500 Andersson, K.M., Kumar, D., Bentzer, J., Friman, E., Ahrén, D., and Tunlid, A. (2014)
501 Interspecific and host-related gene expression patterns in nematode-trapping fungi. BMC
502 Genomics 15: 968.
503
504 Apetri, M.M., Maiti, N.C., Zagorski, M.G., Carey, P.R., and Anderson, V.E. (2006)
505 Secondary Structure of α-Synuclein Oligomers: Characterization by Raman and Atomic Force
506 Microscopy. J Mol Biol 355 : 63–71.
507
508 Baccelli, I., Luti, S., Bernardi, R., Scala, A., and Pazzagli, L. (2014) Cerato-platanin shows
509 expansin-like activity on cellulosic materials. Appl Microbiol Biotechnol 98: 175–184.
510
511 Ball, S.R., Kwan, A.H., and Sunde, M. (2020) Hydrophobin Rodlets on the Fungal Cell Wall
512 Curr Top Microbiol Immunol 425: 29-51.
513
514 Bang, K.H., Lee, D.W., Park, H.M., and Rhee, Y.H. (2000) Inhibition of fungal cell wall
515 synthesizing enzymes by trans-cinnamaldehyde. Biosci Biotechnol Biochem 64: 1061-1063.
516

Belkin, M., and Niyogi, P. (2003) Laplacian eigenmaps for dimensionality reduction and data representation. Neural Comput 15: 1373-1396.

Boucher, C., Nguyen, T.S., and Silar P. (2017) Species delimitation in the *Podospora anserina*/*P. pauciseta*/*P. comata* species complex (Sordariales). Cryptogamie, Mycologie 38: 485-506.

Bouws, H., Wattenberg, A., and Zorn, H. (2008) Fungal secretomes—nature's toolbox for white biotechnology. Appl Microbiol Biotechnol 80: 381-388.

Brun, S., Malagnac, F., Bidard, F., Lalucque, H., and Silar, P. (2009) Functions and regulation of the Nox family in the filamentous fungus *Podospora anserina*: a new role in cellulose degradation. Mol Microbiol 74: 480-96.

Bruneau, M., Mottet, T., Moulin, S., Kerbiriou, M., Chouly, F., Chrétien, S., and Guyeux, C. (2018) A clustering package for nucleotide sequences using Laplacian Eigenmaps and Gaussian Mixture Model. Computers in Biology and Medicine, Elsevier 93: 66-74.

Cao, Y., Zhu, X., Jiao, R., and Xia, Y. (2012) The Magas1 gene is involved in pathogenesis by affecting penetration in *Metarhizium acridum*. J Microbiol Biotechnol 22 : 889–893.

Cock, P.A., Antao, T., Chang, J.T., Chapman, B.A., Cox, C.J., Dalke, A., *et al.* (2009) Biopython: freely available Python tools for computational molecular biology and bioinformatics. Bioinformatics 25: 1422-1423.

Dichtl, K., Helmschrott, C., Dirr, F., and Wagener, J. (2012) Deciphering cell wall integrity signalling in *Aspergillus fumigatus*: identification and functional characterization of cell wall stress sensors and relevant Rho GTPases. Mol Microbiol 83: 506-19.

Dynesen, J., and Nielsen, J. (2003) Surface hydrophobicity of *Aspergillus nidulans* conidiospores and its role in pellet formation. Biotechnol Prog 19: 1049-1052.

Feldman, D., Kowbel, D.J., Glass, N.L., Yarden, O., and Hadar, Y. (2017) A role for small secreted proteins (SSPs) in a saprophytic fungal lifestyle: Ligninolytic enzyme regulation in *Pleurotus ostreatus*. Sci rep 7: 14553.

Feldman, D., Amedi, N., Carmeli, S., Yarden, O., and Hadar, Y. (2019) Manipulating the expression of Small secreted protein 1 (Ssp1) alters patterns of development and metabolism in the white-rot fungus *Pleurotus ostreatus*. Appl Environ Microbiol 85: e00761-19.

Fernández-González, A.J., Valette, N., Kohler, A., Dumarçay, S., Sormani, R., Gelhaye, E., and Morel-Rouhier, M. (2018) Oak extractive-induced stress reveals the involvement of new enzymes in the early detoxification response of *Phanerochaete chrysosporium*. Environ Microbiol 20: 3890-3901.

Frías, M., González, C., and Brito, N. (2011) BcSpl1, a cerato-platanin family protein, contributes to *Botrytis cinerea* virulence and elicits the hypersensitive response in the host. New Phytol 192: 483-495.

566 Futagami, T., Nakao, S., Kido, Y., Oka, T., Kajiwara, Y., Takashita, H., *et al*. (2011) Putative
567 stress sensors WscA and WscB are involved in hypo-osmotic and acidic pH stress tolerance in
568 *Aspergillus nidulans*. Eukaryot Cell 10: 1504-1515.
569
570 Gow, N.A.R., Latge, J.P., and Munro, C.A. (2017) The Fungal Cell Wall: Structure,
571 Biosynthesis, and Function. Microbiol Spectr 5(3).
572
573 Grell, M.N., Mouritzen, P., and Giese, H. (2003) A *Blumeria graminis* gene family encoding
574 proteins with a C-terminal variable region with homologues in pathogenic fungi. Gene 311:
575 181–192.
576
577 Groenning, M. (2010) Binding mode of Thioflavin T and other molecular probes in the
578 context of amyloid fibrils—current status. J Chem Biol 3: 1–18.
579
580 Huang, W., Hong, S., Tang, G., Lu, Y., and Wang, C. (2019) Unveiling the function and
581 regulation control of the DUF3129 family proteins in fungal infection of hosts. Philos Trans R
582 Soc Lond B Biol Sci 374: 20180321.
583
584 Justesen, A., Somerville, S., Christiansen, S., and Giese, H. (1996) Isolation and
585 characterization of two novel genes expressed in germinating conidia of the obligate biotroph
586 *Erysiphe graminis* f. sp. *hordei*. Gene 170: 131–135.
587
588 Kämper, J., Kahmann, R., Bölker, M., Ma, L.J., Brefort, T., Saville, B.J., *et al*. (2006) Insights
589 from the genome of the biotrophic fungal plant pathogen *Ustilago maydis*. Nature 444: 97–
590 101.

Kubicek, C.P., Baker, S.E., Gamauf, C., Kenerley, C.M., and Druzhinina, I.S. (2008) Purifying selection and birth-and-death evolution in the class II hydrophobin gene families of the ascomycete *Trichoderma/Hypocrea*. BMC Evol Biol 8: 4.

Kumar, S., Stecher, G., and Tamura, K. (2016) MEGA7: Molecular Evolutionary Genetics Analysis version 7.0 for bigger datasets. Mol Biol Evol 33: 1870-1874.

Lashuel, H.A., Petre, B.M., Wall, J., Simon, M., Nowak, R.J., Walz, T., and Lansbury, P.T. Jr. (2002) Alpha-synuclein, especially the Parkinson's disease-associated mutants, forms pore-like annular and tubular protofibrils. J Mol Biol 322: 1089-1102.

Linder, M.B. (2009) Hydrophobins: Proteins that self assemble at interfaces. Curr Opin Colloid Interface Sci 14: 356–363.

Luo, J., Wang, K., Li, G.S., Lei, D.Q., Huang, Y.J., Li , W.D., *et al.* (2018) 3,5-Dicaffeoylquinic Acid Disperses Aspergillus Fumigatus Biofilm and Enhances Fungicidal Efficacy of Voriconazole and Amphotericin B. Med Sci Monit 24: 427-437.

Maddi, A., Dettman, A., Fu, C., Seiler, S., and Free, S.J. (2012) WSC-1 and HAM-7 are MAPK-1 MAP kinase pathway sensors required for cell wall integrity and hyphal fusion in *Neurospora crassa*. PLoS ONE 7: e42374.

614 Malavazi, I., Goldman, G.H., and Brown N.A. (2014) The importance of connections between
615 the cell wall integrity pathway and the unfolded protein response in filamentous fungi. Brief
616 Funct Genomics 13: 456-470.
617
618 Meerupati, T., Andersson, K.M., Friman, E., Kumar, D., Tunlid, A., and Ahrén, D. (2013)
619 Genomic mechanisms accounting for the adaptation to parasitism in nematode-trapping fungi.
620 PLoS Genet. 9: e1003909.
621
622 Mitchell, K.M., Zarnowski, R., and Andes, D.R. (2016) Fungal Super Glue: The Biofilm
623 Matrix and Its Composition, Assembly, and Functions PLoS Pathog 12: e1005828.
624
625 Navarro, D., Couturier, M., Damasceno da Silva, G.G., Berrin, J-G., Rouau, X., Asther, M.,
626 and Bignon, C. (2010) Automated assay for screening the enzymatic release of reducing
627 sugars from micronized biomass. Microbial Cell Fact 9: 58.
628
629 Needleman, S., and Wunsch, C. (1970) A general method applicable to the search for
630 similarities in the amino acid sequence of two proteins. J Mol Biol 48 : 443-53.
631
632 Nodet, P., Capellano, A., and Fèvre, M. (1990) Morphogenetic effects of Congo red on
633 hyphal growth and cell wall development of the fungus *Saprolegnia monoka.* J Gen Microbiol
634 136: 303-310.
635
636 Oliphant, T.E. (2006**)** A guide to NumPy, USA: Trelgol Publishing.
637

638 Pazzagli, L., Cappugi, G., Manao, G., Camici, G., Santini, A., and Scala, A. (1999)
639 Purification, characterization, and amino acid sequence of cerato-platanin, a new phytotoxic
640 protein from *Ceratocystis fimbriata* f sp platani. J Biol Chem 274: 24959–24964.
641
642 Pellegrin, C., Morin, E., Martin, F.M., and Veneault-Fourrey, C. (2015) Comparative analysis
643 of secretomes from ectomycorrhizal fungi with an emphasis on Small-Secreted Proteins.
644 Front Microbiol 6: 1278.
645
646 Piotrowski, J.S., Okada, H., Lu, F., Li, S.C., Hinchman, L., Ranjan, A., *et al*. (2015) Plant-
647 derived antifungal agent poacic acid targets b-1,3-glucan. Proc Natl Acad Sci 112: E1490-7.
648
649 Plett, J.M., Kemppainen, M., Kale, S.D., Kohler, A., Legué, V., Brun, A., *et al.* (2011) A
650 secreted effector protein of *Laccaria bicolor* is required for symbiosis development. Curr Biol
651 21: 1197–1203.
652
653 Plett, J.M., Gibon, J., Kohler, A., Duffy, K., Hoegger, P.J., Velagapudi, R., *et al.* (2012)
654 Phylogenetic, genomic organization and expression analysis of hydrophobin genes in the
655 ectomycorrhizal basidiomycete *Laccaria bicolor*. Fungal Genet Biol 49 : 199–209.
656
657 Ragni, E., Fontaine, T., Gissi, C., Latgè, J.P., and Popolo, L. (2007) The Gas family of
658 proteins of *Saccharomyces cerevisiae*: characterization and evolutionary analysis. Yeast 24:
659 297-308.
660
661 Reynolds, D. (2015) Gaussian mixture models. Encyclopedia of biometrics 827-832.

662 Rizet, G. (1941) Sur l'analyse génétique des asques du *Podospora anserina*. C. R. Acad. Sci.
663 Paris 212: 59-61.
664
665 Rizet, G. (1952) Les phénomènes de barrage chez *Podospora anserina*. I. Analyse génétique
666 des barrages entre souches S and s. Rev Cytol Biol Veg 13: 51-92.
667
668 Ruocco, M., Lanzuise, S., Lombardi, N., Woo, S.L., Vinale, F., Marra, R., *et al.* (2015)
669 Multiple roles and effects of a novel *Trichoderma* Hydrophobin. Mol Plant Microbe Interact
670 28: 167–179.
671
672 Schwarz, G.E. (1978) Estimating the dimension of a model. Annals of Statistics 6: 461–464.
673
674 Semerdzhiev, S.A., Lindhoud, S., Stefanovic, A., Subramaniam, V., van der Schoot, P., and
675 Claessens, M.M.A.E. (2018) Hydrophobic-Interaction-Induced Stiffening of Alpha-Synuclein
676 Fibril Networks. Phys Rev Lett 120: 208102.
677
678 Shang, Y., Xiao, G., Zheng, P., Cen, K., Zhan, S., and Wang, C. (2016) Divergent and
679 convergent evolution of fungal pathogenicity. Genome Biol Evol 8: 1374–1387.
680
681 Shanmugam, N., Baker, M.O.D.G., Ball, S.R., Steain, M., Pham, C.L.L., and Sunde, M.
682 (2019) Microbial functional amyloids serve diverse purposes for structure, adhesion and
683 defence. Biophys Rev 11: 287-302.
684
685 Silar, P. (1995) Two new easy-to-use vectors for transformations. Fungal Genet News l 42:
686 73.

687

688 Silar, P. (2013) *Podospora anserina*: from laboratory to biotechnology. In: Genomics of Soil-
689 and Plant-Associated Fungi. P. K. M. Benjamin A. Horwitz, Mala Mukherjee, Christian P.
690 Kubicek (ed). Heidelberg New York Dordrecht London: Springer, pp. 283-309.

691

692 Thuillier, A., Chibani, K., Belli, G., Herrero, E., Dumarçay, S., Gérardin, P., *et al.* (2014)
693 Transcriptomic responses of *Phanerochaete chrysosporium* to oak acetonic extracts: Focus on
694 a new glutathione transferase. Appl Environ Microbiol 80: 6316–6327.

695

696 Tong, S.M., Chen, Y., Zhu, J., Ying, S.H., and Feng, M.G. (2016b) Subcellular localization of
697 five singular WSC domain-containing proteins and their roles in *Beauveria bassiana*
698 responses to stress cues and metal ions. Environ Microbiol Rep 8: 295-304.

699

700 Tong, S.M., Chen, Y., Ying, S.H., and Feng, M.G. (2016a) Three DUF1996 proteins localize
701 in vacuoles and function in fungal responses to multiple stresses and metal ions. Sci Rep 6:
702 20566.

703

704 Tong, S.M., Wang, D.Y., Gao, B.J., Ying, S.H., Feng, M.G. (2019) The DUF1996 and WSC
705 domain-containing protein Wsc1I acts as a novel sensor of multiple stress cues in *Beauveria*
706 *bassiana*. Cell Microbiol 21: e13100.

707

708 Valette, N., Benoit-Gelber, I., Falco, M.D., Wiebenga, A., de Vries, R.P., Gelhaye, E., and
709 Morel-Rouhier, M. (2017) Secretion of small proteins is species-specific within *Aspergillus*
710 sp, Microb Biotechnol 10: 323–329.

711

712 Valette, N., Perrot, T., Sormani, R., Gelhaye, E., and Morel-Rouhier, M. (2017) Antifungal
713 activities of wood extractives. Fungal Biol Rev 31: 113–123.
714
715 Van Den Bossche, H. (2002) Echinocandins - an update. Expert Opinion Ther Pat 12: 151-
716 167.
717
718 Verna, J., Lodder, A., Lee, K., Vagts, A., and Ballester, R. (1997) A family of genes required
719 for maintenance of cell wall integrity and for the stress response in *Saccharomyces cerevisiae*.
720 Proc Natl Acad Sci USA 94: 13804-13809.
721
722 Vincent, D., Kohler, A., Claverol, S., Solier, E., Joets, J., Gibon, J., *et al.* (2012) Secretome of
723 the free-living mycelium from the ectomycorrhizal basidiomycete *Laccaria bicolor*. J
724 Proteome Res 11: 157-171.
725
726 Wessels, J.G., De Vries, O.M., Asgeirsdottir, S.A., and Schuren, F.H. (1991) Hydrophobin
727 genes involved in formation of aerial hyphae and fruit bodies in *Schizophyllum*. Plant Cell 3:
728 793-799.
729
730 Wessels, J.G.H. (1996) Fungal hydrophobins: proteins that function at an interface. Trends
731 Plant Sci 1: 9-15.
732
733 Xue, C., Park, G., Choi, W., Zheng, L., Dean, R.A., and Xu, J.R. (2002) Two novel fungal
734 virulence genes specifically expressed in appressoria of the rice blast fungus. Plant Cell 14:
735 2107-2119.
736

737 Zhang, B., Cai, J., Duan, C.Q., Reeves, M.J., and Fei He, F. (2015) A review of polyphenolics
738 in oak woods. Int J Mol Sci 16: 6978-7014.
739
740 Zhu, N., Liu, J., Yang, J., Lin, Y., Yang, Y., Ji, L., *et al.* (2016) Comparative analysis of the
741 secretomes of *Schizophyllum commune* and other wood-decay basidiomycetes during solid-
742 state fermentation reveals its unique lignocellulose-degrading enzyme system. Biotechnol
743 Biofuels 9: 42.
744
745 Zykwinska, A., Guillemette, T., Bouchara, J-P., and Cuenot, S. (2014) Spontaneous self-
746 assembly of SC3 hydrophobins into nanorods in aqueous solution. Biochemica et Biophysica
747 Acta 1844: 1231-1237.
748
749 **Figure legends**
750 **Fig. 1: Comparative genomics of fungal OSIP1**
751 Sequences were retrieved from the whole fungal JGI database (Mycocosm from Joint
752 Genome Institute) using BlastP search tool with PcOSIP1, PaOSIP1 and P209725 as
753 templates. (A) A total of 1057 sequences have been retrieved (cut off of Evalue=10^{-5}) and
754 clustered as described in Experimental procedures part. The number of sequences found per
755 trophic mode is indicated by various colors for each cluster. (B) Sequence alignment of
756 ascomycete OSIP1 sequences from *P. anserina*, *Chaetomium thermophilum*, *Sordaria*
757 *brevicollis* and *Fusarium solani*. The signal peptide of secretion is colored in yellow, the
758 DUF3129 domain in blue gray. The eight conserved cysteinyl residues are highlighted (in red
759 those that are both conserved in basidiomycete and ascomycete sequences and in orange those
760 that are specifically conserved in ascomycetes sequences) (C) Evolutionary relationship of
761 OSIP1 and DUF3129 containing proteins. The evolutionary history of OSIP1 cluster

762 sequences and DUF3129 containing sequences retrieved from the Pfam database, was inferred
763 using the Neighbor-Joining method. Basidiomycete sequences are highlighted in gray. The
764 functionally characterized proteins are reported. Sc: *Saccharomyces cerevisiae*, Mg:
765 *Magnaporthe grisea*, Pc: *Phanerochate chrysosporium*, Pa: *Podospora anserina*, Bg:
766 *Blumeria graminis*, Cg: *Colletotrichum gloeosporioides*. Because some of DUF3129-
767 containing proteins are annotated as GAS-like proteins in the pfam database, GAS1
768 (Glycolipid Anchored Surface) from *Saccharomyces cerevisiae* that has been well studied
769 (Ragni *et al*., 2007) and the GAS1 sequence of *P. chrysosporium*, were added to the analysis.
770
771 **Fig. 2: Growth phenotype of *PaOSIP1*$^{\Delta}$ in presence of caspofungin.**
772 Wild type, *PaOSIP1*$^{\Delta}$ mutant and a complemented strain (*PaOSIP1*$^{\Delta}$*_PaOSIP1)* were grown
773 in M2 medium as control (A) and M2 supplemented with caspofungin (500 ng/ml) (B) for 10
774 days at 27°C (n=3). The pictures show fungal growth after 10 days.
775
776 **Fig. 3: SEM images of *PaOSIP1*$^{\Delta}$ and WT hyphal network.**
777 Cryosections of mycelium were obtained as described in material and methods and visualized
778 by scanning electron microscopy. Images shown in the figure correspond to the top left
779 quarter of the whole images shown in supplemental data. The bar scale corresponds to 5 µm.
780 The extracellular matrix has been manually colored in yellow, the merged images are shown
781 in the middle panels. The single colored ECM is presented on the right panels.
782
783 **Fig. 4: Self-assembly of PcOSIP1.**
784 (A) Circular dichroïsm analysis of PcOSIP1 secondary structure. The spectrum was recorded
785 in 50 mM phosphate buffer pH 8.0 with 66 µM of protein. PcOSIP1 spectrum shows signals
786 at 190, 208 and 222 nm (B) Dynamic light scattering analysis of the oligomerization state of

PcOSIP1. The percentage of the various oligomers of PcOSIP1 in 30 mM Tris-HCl pH 8.0-200 mM NaCl buffer (Tris-NaCl buffer) and 50 mM phosphate buffer pH 8.0 (Phosphate buffer) is represented by black bars. Rh: hydrodynamic radii. (C) Atomic Force Microscopy height images of PcOSIP1 in Tris-NaCl buffer and Phosphate buffer. Size of AFM images: 3 µm × 3 µm. (D) Macromolecular (1 and 2) and microscopic (3) views of the PcOSIP1 gel.

Fig. 5: Growth phenotype of *PaOSIP1*$^{\Delta}$ in presence of oak extractives.

Growth kinetics of the wild type, *PaOSIP1*$^{\Delta}$ mutant and a complemented strain (*PaOSIP1*$^{\Delta}$*_PaOSIP1)* in M2 medium supplemented with oak extractives (2 mg/ml) (n=3). The pictures show fungal growth after 10 days.

Fig. 6: Secretome analysis of *PaOSIP1*$^{\Delta}$ in comparison to the wild type strain in presence of oak sawdust.

(A) Global analysis of the amount of proteins specifically detected or more abundant ((PAI) fold>2) in the secretome of each strain in presence of oak sawdust (the experimental set up is described in the experimental section). (B) Percentage of the proteins found specific or more abundant in *PaOSIP1*$^{\Delta}$ within the total of the proteins identified for each functional class. (C) Number of glycoside hydrolases (GH) of each family detected in the secretomes of *PaOSIP1*$^{\Delta}$ and wild type strains in presence of oak sawdust. The proportion of proteins detected as specific or more abundant (PAI fold>2) in the mutant strain is represented as red bars, the dark blue bars corresponding to the number of GH showing PAI fold<2 for the mutant compared to wild type. (D) Protein Abundance Index (PAI) for each strain. A focus has been made on cell wall-related proteins. ProtID are those from the JGI Mycocom database. Full proteomic data are available in Table S2.

Fig S1: Sequence alignment of basidiomycete OSIP1 sequences from *P. chrysosporium, T. versicolor, Phlebiopsis gigantea, Punctularia strigosozonata* and *Phlebia centrifuga.* The signal peptide of secretion is colored in yellow, the DUF3129 domain in blue gray. The four conserved cysteinyl residues are highlighted in red.

Fig. S2: Strategy for PaOSIP1 deletion. (A) Gene replacement strategy for deleting *PaOSIP1* in *Podospora anserina*. (B) Primers used for gene replacement and probe synthesis as described in the experimental procedures section. (C) Southern blot showing the efficiency of the gene replacement and insertion of the resistance cassette in a single copy within the genome. Genomic DNA was digested by Pst1 restriction enzyme and hybridized with both AB and CD digoxigenin labeled probes.

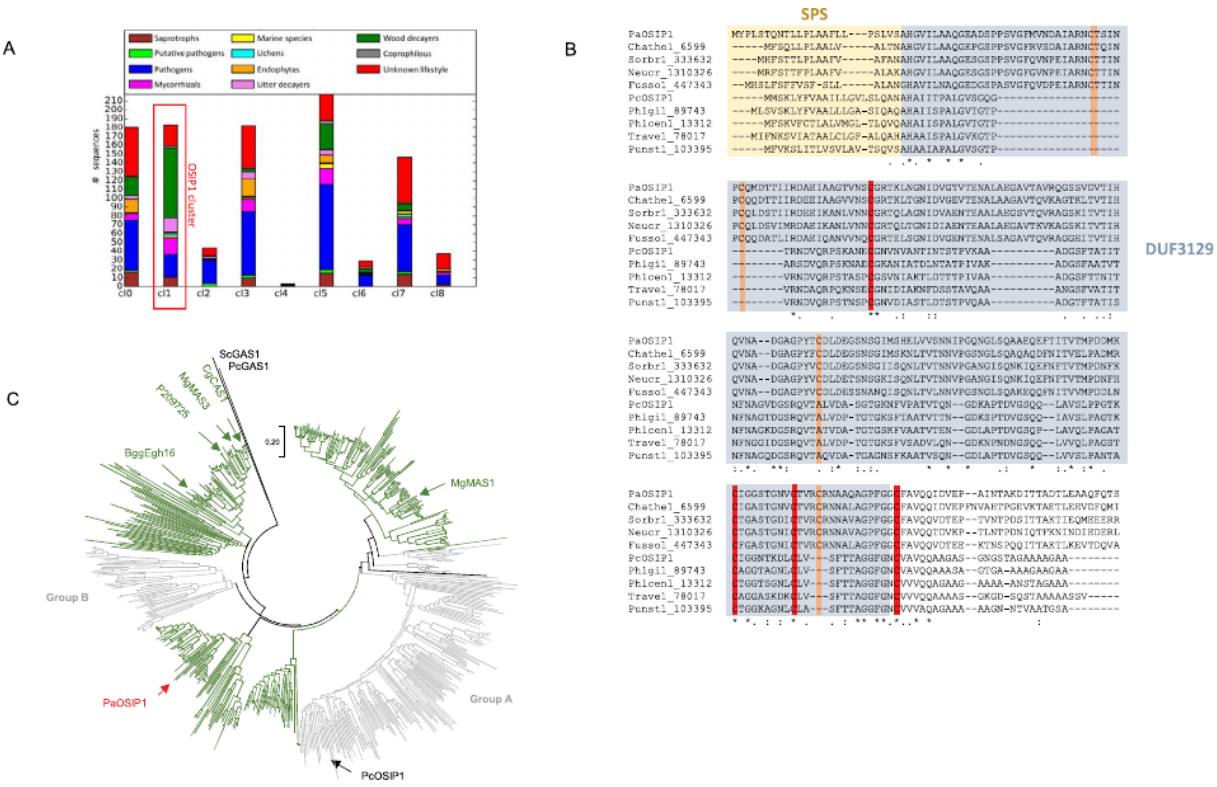

Figure 1

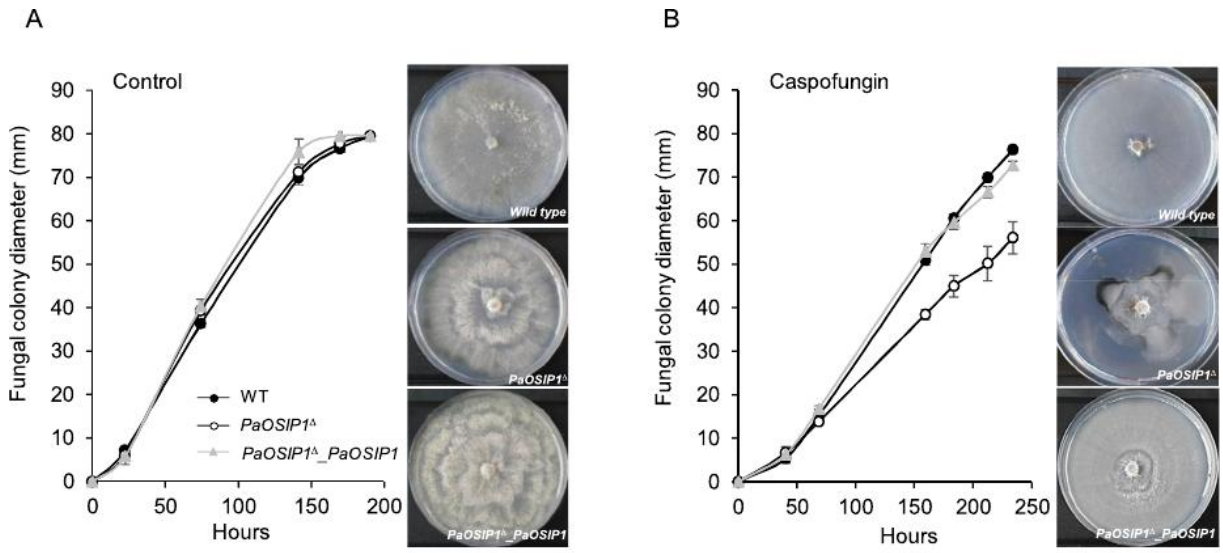
A
Control
Fungal colony diameter (mm)
Hours
WT
PaOSIP1Δ
PaOSIP1Δ_PaOSIP1
Wild type
PaOSIP1Δ
PaOSIP1Δ_PaOSIP1
B
Caspofungin
Fungal colony diameter (mm)
Hours
Wild type
PaOSIP1Δ
PaOSIP1Δ_PaOSIP1

Figure 2

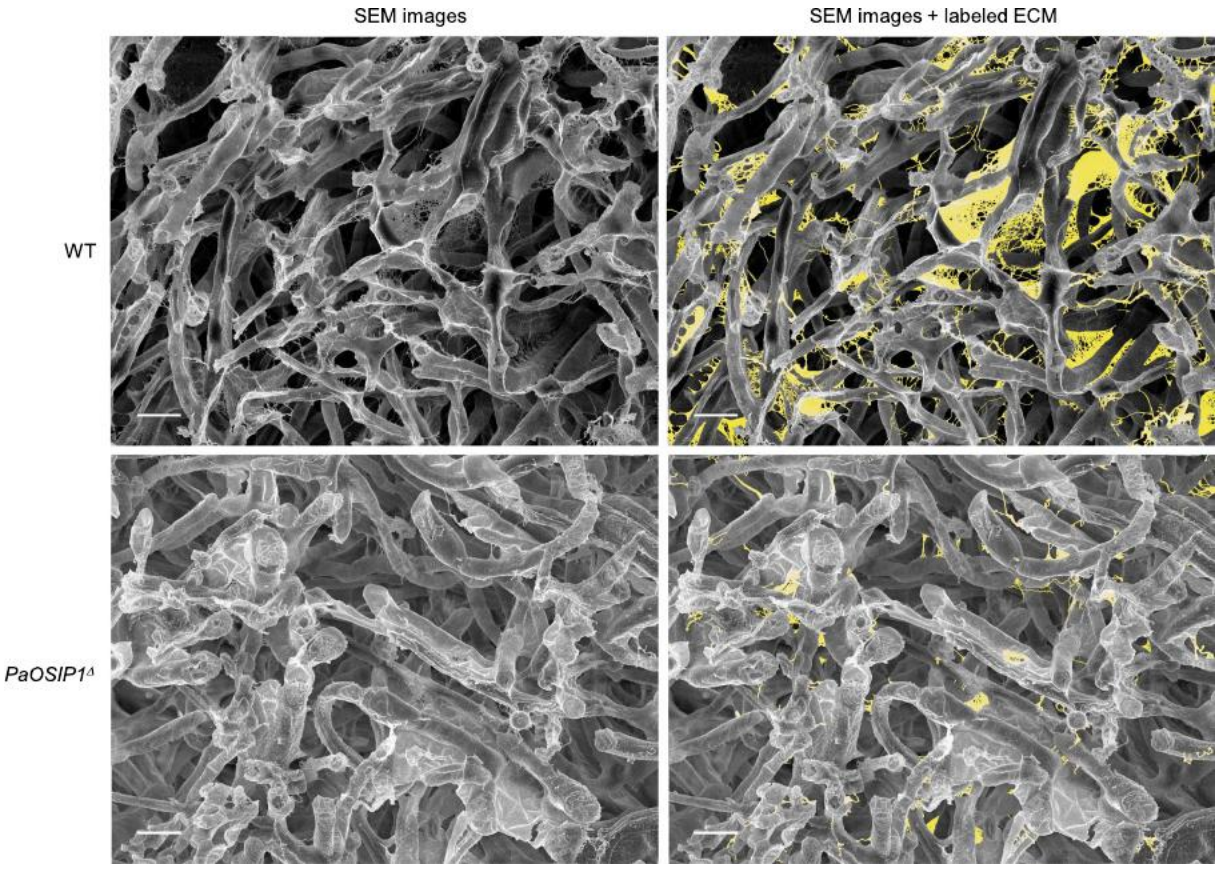
SEM images
SEM images + labeled ECM
WT
PaOSIP1Δ

834 **Figure 3**

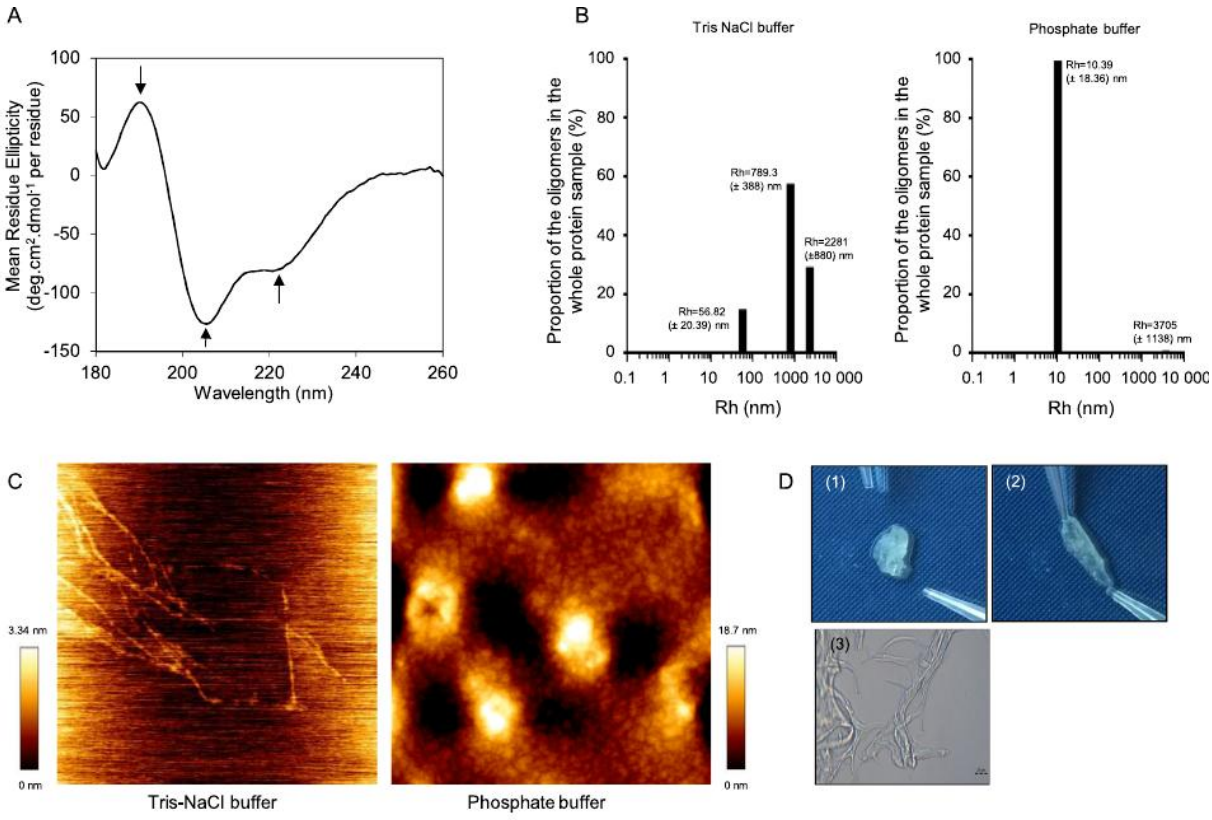

835

836 **Figure 4**

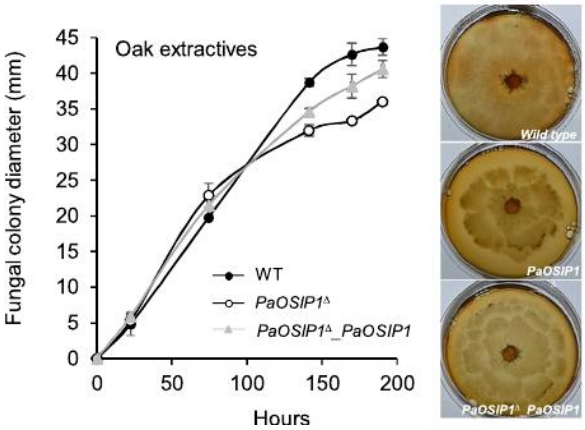

837

838 **Figure 5**

839

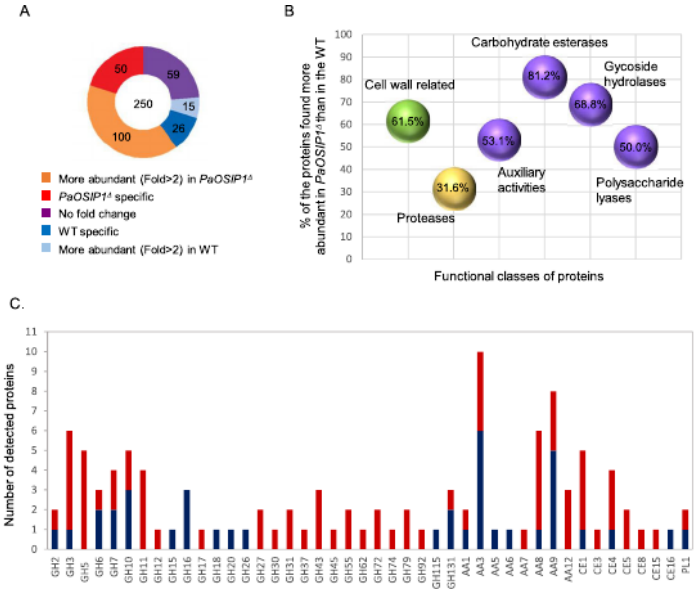

D.

PAI		Fold	ProtID	Putative annotation
WT	*PaOSIP1*Δ			
0.00	1.33	>	210732	hypothetical cell wall protein
0.00	0.77	>	205788	GH17 (glucan-acting enzyme)
0.00	0.50	>	207368	CE8 (pectinesterase)
0.00	0.50	>	201566	cell wall β-glucan synthesis protein
0.33	1.60	4.85	211001	GH131 (β-glucanase)
1.00	3.50	3.50	211650	WSC containing protein
0.17	0.50	3.00	203648	hypothetical cell wall mannoprotein
1.75	4.50	2.57	210664	hypothetical surface protein
0.18	0.41	2.33	204303	GH72 (β-1,3 glucanosyltransferase)
0.45	0.91	2.00	205236	GPI-anchored cell wall protein
0.29	0.57	2.00	206739	GH7 (β-glucanase)
0.06	0.12	2.00	206357	GH72 (β-1,3 glucanosyltransferase)
0.67	1.25	1.87	209105	hypothetical/wall associated proteinase
0.50	0.87	1.75	202082	GH131 (β-glucanase)
1.25	2.00	1.60	206552	GH131 (β-glucanase)
1.93	2.79	1.44	206868	hypothetical/non-anchored cell wall protein
1.09	0.45	0.42	210253	WSC containing protein
0.14	0.00	<	211393	WSC containing protein

Figure 6